

Ping Xu¹, Quanxu Mu¹, Weining Zhang¹

¹AVIC Shenyang Aircraft Design and Research Institute, Shenyang, 110035, China

Abstract

The structural design of the aircraft leading edge faces great challenges due to extreme aerodynamic heating and high-pressure loads. This study aims to enhance the load-bearing and heat dissipation capabilities of the aircraft leading edge by integrating lattice structures and cooling channels. The specific stiffness and thermal conductivity of three lattice structures including simple cubic (SC), body-centered cubic (BCC) and face-centered cubic (FCC) with three flow channel cross-section shapes of rectangle, triangle and semicircle were evaluated, and the asymptotic homogenization method was applied to simplify the finite element analysis and ensure computational efficiency. A response surface model was developed to optimize the lattice design parameters to balance mechanical and thermal performance. In addition, a topology optimization model for the layout of cooling channels was proposed to enhance heat dissipation and ensure uniform temperature distribution. Simulation verification shows that the optimized multi-scale leading edge structure performs well in terms of specific stiffness and heat dissipation efficiency. The proposed design framework effectively addresses the dual challenges of mechanical load-bearing and thermal management, which helps to improve the safety and service life of the aircraft.

Keywords: leading edge; lattice structure; active cooling; thermal protection

1. Introduction

This sample article is to show you how to prepare and submit papers in a standard style for electronic publishing in the ICAS 2024 proceedings. It illustrates the paper layout, and describes points you should notice before you submit your papers.

The papers will be in A4 size with margins top 30 mm, left and right 17.5 mm, bottom 22 mm. The text should be Helvetica with font size 11 point.

Hypersonic aircraft refers to aircraft that fly at speeds greater than Mach 5. When a hypersonic aircraft flies, the airflow friction is severe, causing the surrounding air temperature to rise sharply. Heat is continuously transferred from the air to the aircraft, and is subject to severe air friction heat, resulting in aerodynamic heat problems [1]. Under the condition of huge aerodynamic heat load, the potential temperature of the sharp leading edge stagnation area can exceed 2200K. This high temperature will have a serious impact on the materials of the aircraft, which may cause thermal expansion, oxidation, embrittlement or failure of the materials. Special high-temperature materials or cooling systems are required to deal with these problems. At the same time, lightweight characteristics are an important performance of an aircraft. How to ensure that the leading edge structure has sufficient stiffness, strength and fatigue resistance while keeping the weight low is also an issue that needs to be considered.

As a periodic structure, the lattice structure has good designability and can be designed differently according to different structural functions to resist higher stress, so it is more suitable for working under the combined action of mechanical and thermal loads [2]. Compared with open-cell metal foams with randomly arranged pore structures, the lattice sandwich structure with periodic unit cells has a core deformation dominated by rod stretching under mechanical loads, so it has a better specific strength/stiffness at the same porosity [3]. In view of the heat dissipation performance of the lattice structure, Khaderi et al. [4] simplified the equal cross-section model of the Gyroid lattice and calculated its equivalent thermal conductivity. Valdevit et al. [5] optimized the design of various lattice structures based on mechanical and thermal conductivity properties, and found that the hexagonal structure had the best comprehensive performance; Moon et al. [6] compared Kagome, pyramid, and diamond lattices with the goal of load-bearing capacity and lightweight, and pointed out that the Kagome lattice had the best performance and applied it to unmanned aerial vehicle wing. Active cooling is a cooling method that carries the cooling fluid itself or obtains cooling fluid from the outside to exchange heat with the wall to take away heat or form a gas film to cover the high-temperature wall surface to prevent heat transfer [7,8]. Compared with traditional insulation structures, the active cooling concept proposed by Becher et al. [9] has a better cooling effect. Wieting et al. [10] carried out the overall structural design of the scramjet engine based on the NASA scramjet engine model. The results showed that the overall design goal of a Mach number of less than 9 can be achieved by using active cooling wall plates; Scotti et al. [11] used a simplified analytical model to optimize the design of cooling channels with the goal of minimizing the amount of coolant. The design results met the constraints of structural stress, coolant temperature and pressure drop. Youn et al. [12] proposed an analytical model for the heat transfer of incompressible flow in rectangular pipes. By analyzing the sensitivity of mass flow to various design variables, the minimum mass flow of a single cooling channel was obtained. At present, most leading edge structures adopt improved structures and materials to cope with high-temperature thermal loads, and rarely use active cooling designs. Microtruss structures have not been effectively applied to aircraft leading edges. From the above analysis, it can be found that combining active cooling and lattice structures is a potential effective means to achieve high-performance aircraft leading edge structures.

Against the above background, this paper combines active cooling channels with lattice structures and establishes a systematic leading edge structure design process to improve the load-bearing capacity and heat dissipation capacity of the aircraft leading edge. This study aims to enhance the load-bearing and heat dissipation capabilities of the leading edge through the use of lattice structures and cooling channels. Analyze different lattice types and cooling channel shapes for optimal performance. Size and topology optimization methods, combined with response surface models and multi-objective optimization, improve the thermal and mechanical performance of the design. Simulation results validate the optimization model and prove the effectiveness of the proposed

design method.

2. Optimization method for aircraft leading edge structure

2.1 General idea

The papers should be prepared, if possible, using the format like this document.

The schematic plan view of the front edge structure including micro trusses and flow channels is shown in Figure 1. The front edge can generally be regarded as being made up of two flat plates spliced at a certain angle. The outermost side is the fluid area, and the flow is opened in the solid wall plate. road. The inlet pipe leads from one side to the front edge end, and the outlet pipe is located behind the other side and is formed by the intersection of the upper and lower pipes. After the coolant enters the front edge from the inlet, it flows out from the outlet through the internal flow channel of the wall plate. The inside of the leading edge is a micro-truss area, in which evenly arranged micro-truss unit cells are embedded.

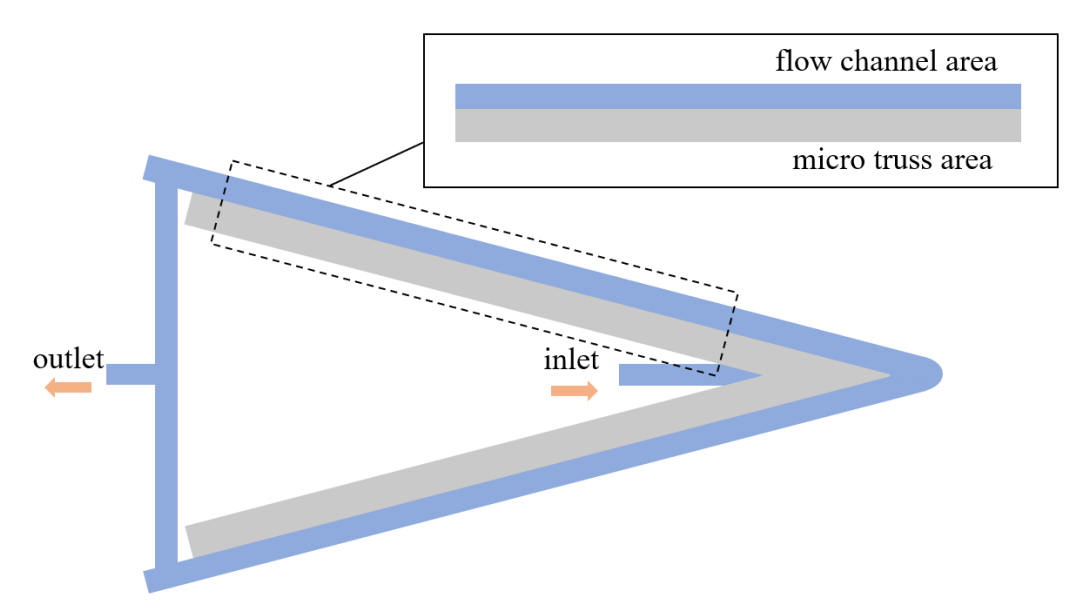


Figure 1 – Schematic diagram of the leading edge structure with micro-trusses and flow channels.

The design idea of this article is shown in Figure 2. First, the asymptotic homogenization method is used to establish a rapid analysis method for fluid-solid thermal simulation. Use this analysis method to perform mechanical and thermal simulation analysis on the combination of three microtruss types and three flow channel cross-sectional shapes, compare the mechanical properties and heat dissipation performance of each scheme, and obtain the optimal micro-truss configuration and flow channel cross-sectional shape. Based on the response surface method, the relationship between temperature, stiffness and various dimensional parameters is fitted, and then the NSGA-II multi-objective genetic optimization algorithm is used to optimize the parameters of the optimal micro-truss configuration. The flow channel section selects the optimal shape, the heat dissipation effects of several flow channel layouts are compared, and the flow channel layout is reasonably designed through topology optimization. Finally, the leading edge structure containing the flow channel and the micro-truss is integrated and modeled, and the reliability of the model is verified by simulation.

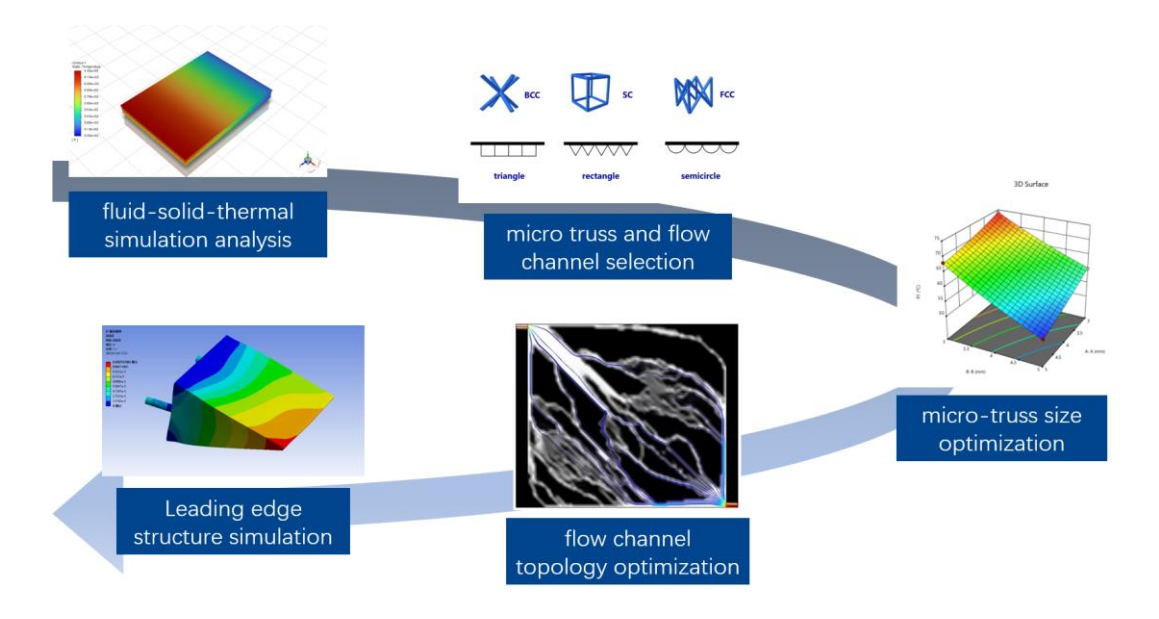


Figure 2 – Design ideas of this paper.

2.2 Numerical model

The simulation calculation problem considered in this article is the fluid heat transfer problem, and the governing equations are the mass conservation equation, the momentum conservation equation and the energy conservation equation [13]. The solid domain energy equation is also solved and represented by equation (4), where Q_{in} represents the heat source value applied to the model.

$$\nabla \cdot \rho \vec{V} = 0 \tag{1}$$

$$\nabla \cdot \rho \vec{V} \vec{V} = -\nabla p + \nabla \tau \tag{2}$$

$$\nabla \cdot \left(\rho c_p \vec{V} T\right) = k \nabla^2 T \tag{3}$$

$$k_s \nabla^2 T = Q_{in} \tag{4}$$

In the formula, represents fluid density, V represents fluid velocity, cp represents fluid specific heat capacity, k represents fluid thermal conductivity, ks represents solid thermal conductivity, p represents fluid pressure, T represents flow stress tensor, and T represents temperature.

In the selection and optimization of the lattice and flow channels, in order to simplify the calculation, the wall plate on one side of the leading edge was extracted for analysis. One side of the solid wall panel at the front edge of the aircraft receives a heat source of about 10 kW/m², with a temperature as high as 600°C. The other side is in contact with 300K normal temperature air, and the convection heat transfer coefficient is 20 W/(m²·K). By conducting heat transfer simulations on solid wall panels, it can be estimated that the heat flux value when the temperature of the wall panel contact heat source surface reaches 600°C is 11kW/m². The fluid channel is evenly filled with No. 65 coolant, the total flow rate is 90ml/min, and the inlet temperature is 300K.

This article also considers the bearing problem of the structure, and the control equation is as follows:

$$KU = F \tag{5}$$

U and F are displacement and force respectively, and K is stiffness.

The solid material is a nickel-based high-temperature alloy, the bottom surface is fixed and constrained, and a displacement load of 0.5mm in downward direction is applied to the top surface.

2.3 Asymptotic homogenization (AH) method

On the microscopic scale, the asymptotic homogenization method is used to calculate the macroscopic equivalent elastic modulus and equivalent thermal conductivity matrix of the microstructure [14]. The specific calculation expressions are as follows:

$$\mathbf{D}^{H} = \frac{1}{|Y|} \int_{V} \left[\mathbf{D}(\mathbf{y}) - \mathbf{D}(\mathbf{y}) \varepsilon_{y}(\chi, \mathbf{y}) \right] d\mathbf{y}$$
 (6)

$$\lambda^{H} = \frac{1}{|Y|} \int_{Y} \left[\lambda(\mathbf{y}) - \lambda(\mathbf{y}) \varepsilon_{y}(\kappa, \mathbf{y}) \right] d\mathbf{y}$$
 (7)

Among them, χ , κ are two sets of eigenvectors, which are obtained by calculating the following three control equations when periodic boundary conditions are imposed:

$$\int_{V} \varepsilon_{y}^{T}(\mathbf{v}) \left[\mathbf{D}(\mathbf{y}) - \mathbf{D}(\mathbf{y}) \varepsilon_{y}(\chi) \right] d\mathbf{y} = 0, \forall \chi \in V_{y}$$
(8)

$$\int_{\mathbf{y}} \varepsilon_{\mathbf{y}}^{\mathrm{T}}(\mathbf{v}) \left[\lambda(\mathbf{y}) - \lambda(\mathbf{y}) \varepsilon_{\mathbf{y}}(\kappa) \right] d\mathbf{y} = 0, \forall \kappa \in V_{\mathbf{y}}$$
(9)

Among them, $V_y = \{u_y(\mathbf{y}) | \mathbf{y} \in Y, u_y(\mathbf{y} + Y) = u_y(\mathbf{y})\}$ represents the function space of the periodic function defined in the unit cell domain, and \mathbf{v} represents the virtual displacement field.

The side length and height of the bottom surface of the micro-truss unit are not guaranteed to be consistent. After being homogenized into a solid structure, it is an orthotropic material. The stiffness matrix D of this material is calculated by formula (13). Using a simple cubic cell with a bottom side length of 5 mm, a height of 4 mm, and a rod diameter of 1 mm, a rectangular flow channel model is used as a typical sample to calculate the D matrix of this type of cell. The number of grids directly divided into this model is 7441146. After homogenization, the number of model grids is 76700. The number of grids is reduced to about 1% of the original number, which greatly improves the calculation efficiency. A schematic diagram comparing the direct meshing and the model mesh after homogenization is shown in Figure 3.

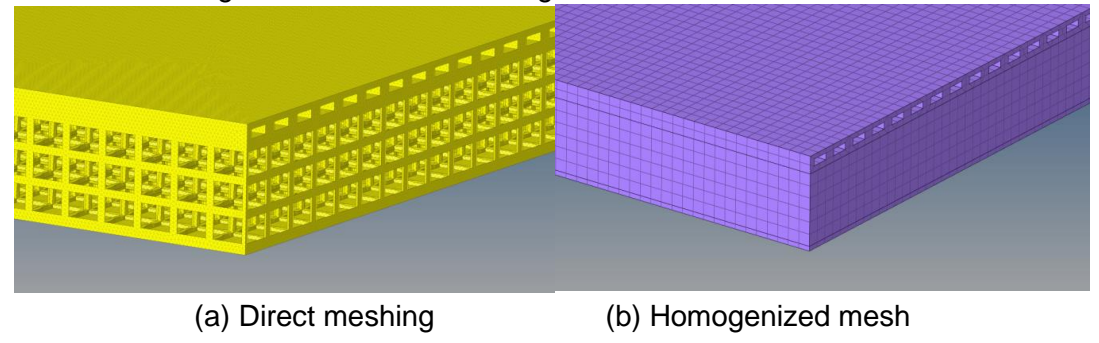
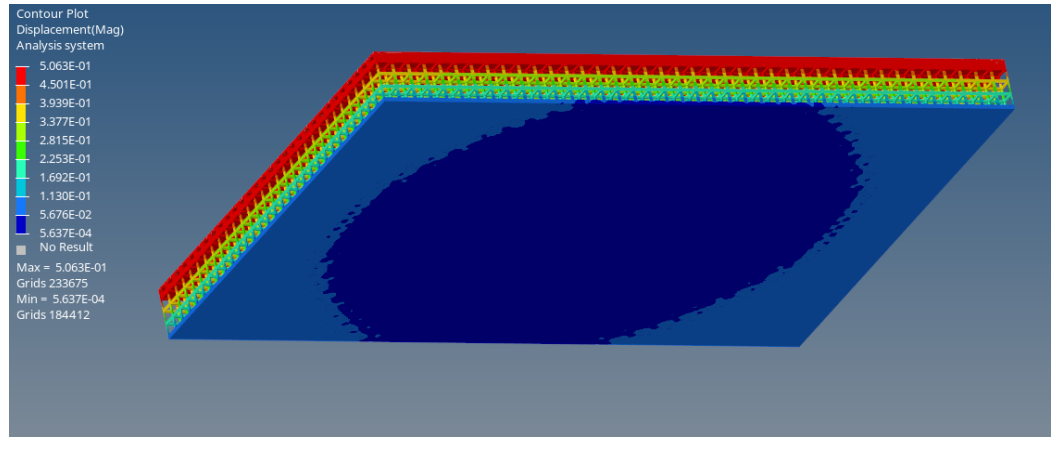


Figure 3 – Comparison between direct meshing and homogenized model meshing in mechanical calculations.

The y direction of the bottom surface is fixed, and a 0.5mm displacement load is applied to the top surface. The comparison of the deformation cloud diagrams of the accurate model and the homogenized model is shown in Figure 4. The total reaction force calculated by the precise mesh model is 4506151N, and the stiffness is 9012302N/mm; the total reaction force calculated by the homogenized model is 4443171N, and the stiffness is 8886342N/mm. The difference between the two results is only 1.4%, indicating that the homogenized model still maintains a high calculation accuracy.



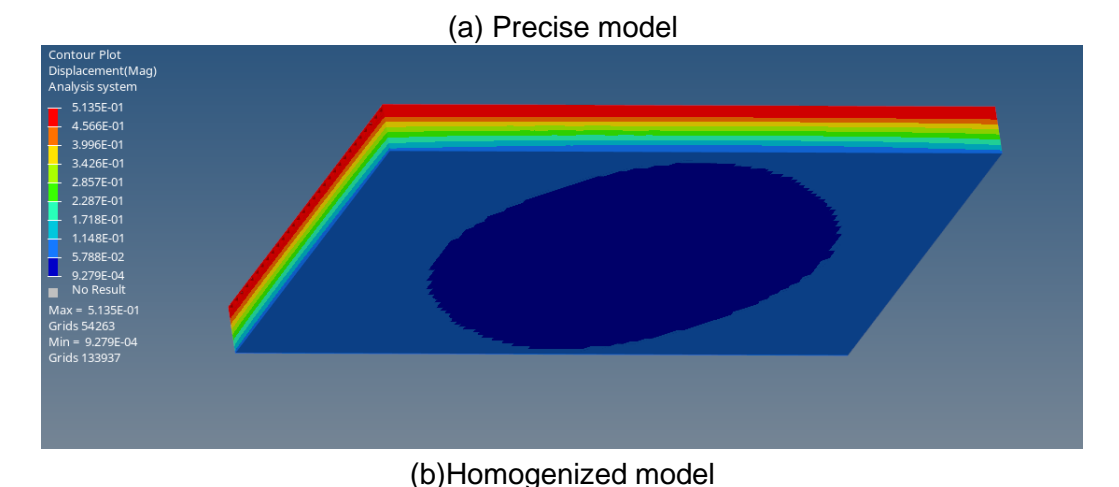


Figure 4 – Deformation cloud diagram of precise model and homogenized model.

The equivalent heat transfer coefficient matrix λ after homogenization is calculated by formula (6). Using a simple cubic cell with a bottom side length of 5 mm, a height of 4 mm, and a rod diameter of 1 mm, a rectangular flow channel model is used as a typical sample to calculate the λ matrix of this type of cell. The number of directly divided meshes is 5930997, and the number of model meshes after homogenization is 542909. The number of meshes is reduced to about 9% of the original number, which greatly improves the calculation efficiency. A schematic diagram comparing the direct meshing and the model mesh after homogenization is shown in Figure 5.

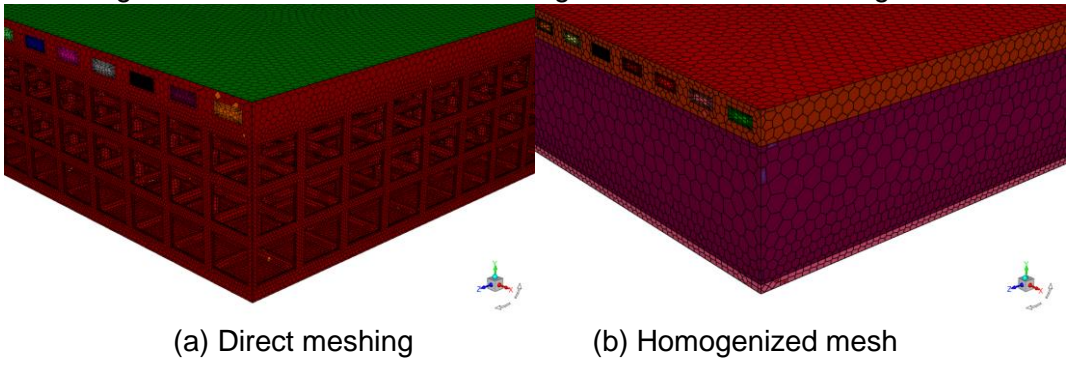
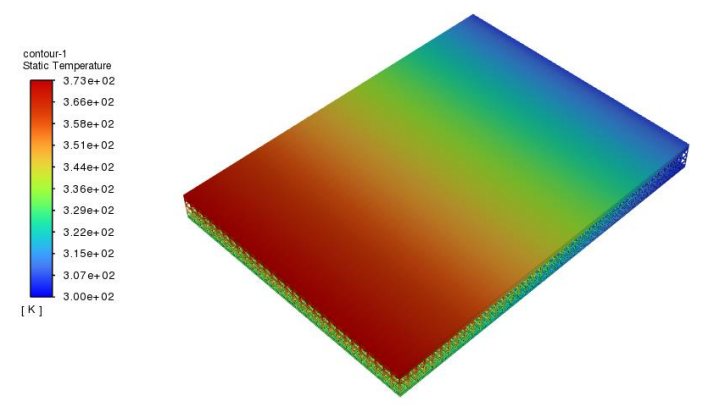


Figure 5 – Comparison between direct meshing and homogenized model meshing in heat transfer calculations.

The size of the heat source on the top surface is 11kw/m2, and the convection heat transfer coefficient between the bottom surface and the 300K air is 20 W/(m²·K). Each flow channel is filled with No. 65 coolant and has the same flow rate. The comparison of the deformation cloud diagrams of the precise model and the homogenized model is shown in Figure 6. The precise grid model calculated the maximum temperature of the structure at 372.8K, and the homogenized model calculated the maximum temperature of the structure at 373.1K. The difference between the two results was only 0.08%, indicating that the homogenized model still maintained a high calculation accuracy.



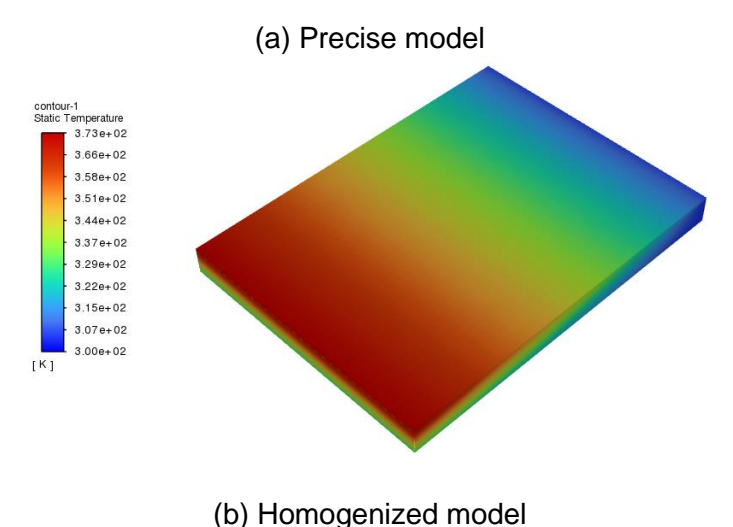


Figure 6 – Temperature cloud diagram of precise model and homogenized model.

2.4 Heat transfer model with Darcy flow

The flow problem inside the flow channel is modeled using the incompressible steady-state Navier-Stokes equation:

$$\rho \mathbf{u} \cdot \nabla \mathbf{u} = -\nabla P + \mu \nabla^2 \mathbf{u} - \rho \mathbf{b} \tag{10}$$

$$\nabla \cdot \mathbf{u} = 0 \tag{11}$$

In the formula, u represents the velocity field, P represents the pressure, μ is the dynamic viscosity, ρ is the mass density, and the vector b is the body force per unit mass.

This flow velocity field can be solved by the Darcy seepage model [15]. The velocity field of the Darcy model can be expressed as:

$$\mathbf{u} = \frac{\kappa}{\mu} \nabla \mathbf{P} \tag{12}$$

Among them, κ is the permeability, which determines the position of solids and fluids in the model. According to the velocity field obtained by the Darcy model, a convection-diffusion heat conduction model is established to solve the temperature field:

$$\rho c_n \mathbf{u} \cdot \nabla T = k \nabla^2 T + Q \tag{13}$$

Substituting formula (13) into the equation, we can get the following form:

$$\rho c_p \left(-\frac{\kappa}{\mu} \nabla P \right) \cdot \nabla T = k \nabla^2 T + Q \tag{14}$$

Among them, T is the temperature field, k is the thermal conductivity, cp is the specified heat, and Q is the volumetric heat source intensity.

3. Results

3.1 Micro truss and flow channel selection

There are three types of micro-truss types studied in this article, namely SC type, BCC type, and FCC type, as shown in Figure 7. There are three types of flow channel configurations, namely rectangle, semicircle, and triangle, as shown in Figure 8. The BCC cell is a body-centered cubic unit with strong shear resistance and large stiffness in the diagonal direction; the SC cell is a simple cubic unit with the largest Young's modulus along the axial direction and has Super stiffness in the axial direction; FCC cells are face-centered cubic cells, which are more balanced and have better stability under complex stresses. The combination of different unit cell types and flow channel shapes has different volume ratios, stiffness and heat dissipation capabilities.

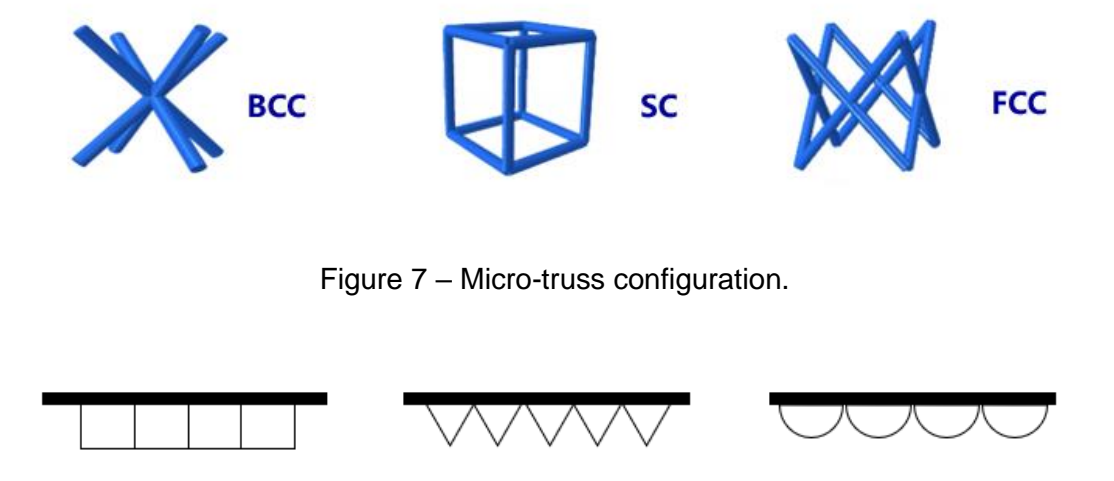


Figure 8 – Flow channel configuration.

rectangle

semicircle

triangle

When preparing the test piece, the minimum size constraint for additive manufacturing is 0.8 mm. The size of a single cell is limited to 3~5mm. The influence of cell size on flat specimens mainly has two aspects, one is along the plane direction, and the other is along the thickness direction. The cell under study is a rectangular parallelepiped with a square bottom surface. The side length of the cell bottom surface is initially set to 5mm, the cell height is set to 4mm, and the micro-truss rod diameter is set to 1mm. Three unit cell configurations and three flow channel shapes are set. The combination arrangement forms 9 structural types, as shown in Figure 9. The nine configuration schemes are rectangular flow channel plus SC cells, rectangular flow channel plus BCC cells, triangular flow channel plus SC cells, triangular flow channel plus SC cells, semicircular flow channel plus FCC cells, and semicircular flow channel plus FCC cells.

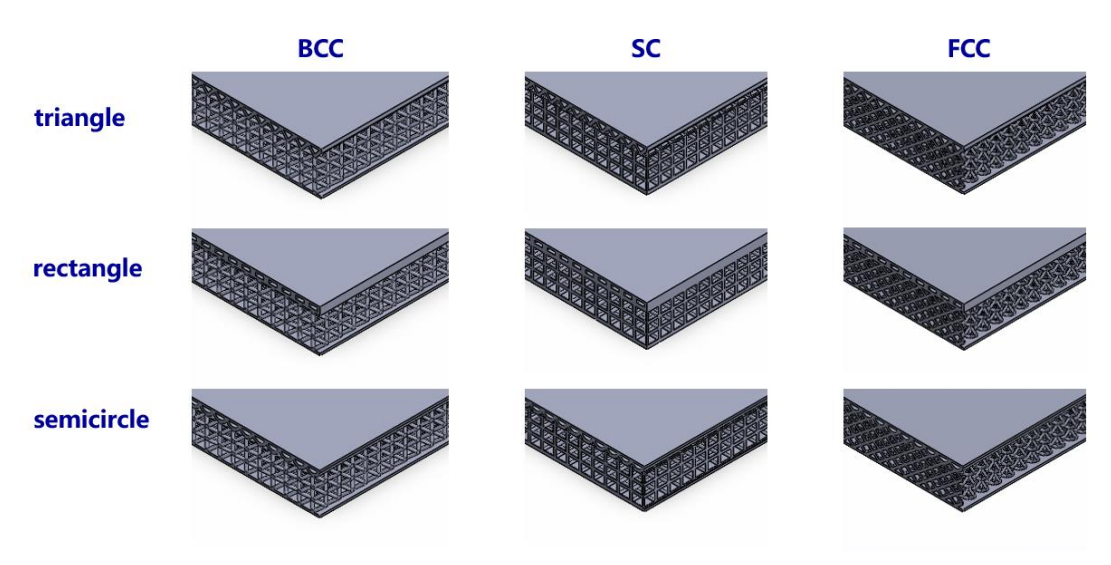


Figure 9 – Combination schemes of different flow channels and micro-trusses.

Using the thermal-fluid-solid coupling simulation analysis method established in this project, compression simulation and active cooling simulation were performed on these nine combination schemes to obtain the stiffness and specific stiffness of different combinations, the maximum temperatures of the cold and hot surfaces at the same flow rate, and the volume ratio of each

component was calculated. The data are shown in Tables 1-5.

Table 1 – Stiffness of each configuration.

Tubi	c i Cililiooo c	Other Cool of Cach Cornigaration.		
Stiffness(N/m	m) BCC	SC	FCC	
triangle	6183105	4340490	11694084	
rectangle	5948086	9012302	10958630	
semicircle	6535670	6340902	11745988	

Table 2 – Specific stiffness of each configuration.

Specific stiffness (N/mm/g)	BCC	SC	FCC
triangle	8553.207113	7960.05	17877.9
rectangle	7973.601587	15847.9	16175.1
semicircle	9212.48022	11897.2	18311.6

Table 3 – Maximum temperature of cold surface of each configuration.

maximum temperatures of the cold surface (°C)	BCC	SC	FCC
triangle	116	86	114
rectangle	116	99	113
semicircle	118	89	115

Table 4 – Maximum temperature of hot surface of each configuration.

maximum temperatures of the cold surface (°C)	BCC	SC	FCC
triangle	154	167	161
rectangle	152	158	159
semicircle	154	169	165

Table 5 – The volume ratio of each configuration.

Volume fraction (%)	BCC	SC	FCC
triangle	32.9	24.82	29.77
rectangle	35.05	26.72	32.57
semicircle	33.52	25.18	30.31

By comparing the mechanical and thermal properties of the above nine configurations, it is known that the rectangular flow channel plus SC cells simultaneously meet good load-bearing, lightweight and heat dissipation capabilities. The hot surface is less than 160° C, the cold surface is less than 100° C, and the specific stiffness is greater than 15000 N/mm/g. Next, the configuration scheme of a combination of rectangular flow channel and SC cells will be selected for analysis and optimization.

3.2 Micro-truss size optimization

This article intends to optimize the unit cell height A, unit cell bottom side length B, and micro-truss rod diameter C. Its design variables are:

$$x = [x_1, x_2, x_3]^T = [A, B, C]^T$$
(15)

The design goals are to ensure the load-bearing capacity and the maximum heat exchange capacity of the structure under the requirement of lightweight structure. The load-bearing capacity is represented by the stiffness R3, and the heat transfer capacity is represented by the maximum

temperature of the cold surface R1 and the maximum temperature of the hot surface R2. Multiobjective optimization is performed on these three objectives, and the objective function is expressed as:

$$\begin{cases}
Min: R1(x), R2(x) \\
Max: R3(x)
\end{cases}$$
(16)

During the iterative optimization process toward the objective function, the following constraints must be met:

$$\begin{cases} 3 \le A \le 5 \\ 3 \le B \le 5 \\ 0.8 \le C \le 1 \end{cases}$$

$$\frac{V(x)}{V_0} \le 35\%$$

$$(17)$$

The constraints in the above formula are the unit size constraints after considering the additive manufacturing process, and the structural lightweight rate. The acquisition of test data sample points is calculated through the control equation. The unit size constraints are the lower limit of the unit bottom side length 3mm and the upper limit 5mm; the lower limit of the unit height is 3mm and the upper limit 5mm; the lower limit of the micro-truss rod diameter is 0.8mm and the upper limit 1mm. The structural lightweight rate is less than 35% of the overall volume fraction of the thermal protection unit.

The polynomial response surface method is a method that combines experimental design and mathematical statistics related theories to construct a surrogate model, and is widely used in nonlinear optimization problems such as contact-collision [16]. The main principle of constructing a polynomial response surface model based on the polynomial response surface method is to express the complex implicit functional function in an explicit polynomial form, and then find the global optimal solution of the polynomial through an optimization method [17].

In the process of optimizing the multi-dimensional parameters of the micro-truss structure unit cell, the unit cell height A, the unit cell bottom side length B, and the micro-truss rod diameter C are used as design variables. The maximum temperature of the cold surface R1, the maximum temperature of the hot surface R2, the structure The stiffness R3 and volume fraction R4 are used as response values, and the Box-Behnken experimental design method is used to establish and analyze the response surface.

Box-Behnken experimental factors and levels are shown in Table 6, and experimental results and analysis are shown in Table 7.

Table 6 – Experimental factors and levels of microtruss parameter optimization.

Factor	-1	0	1
Unit cell height A/mm	3	4	5
Unit cell base side length B/mm	3	4	5
Micro truss rod diameter C/mm	8.0	0.9	1

Table 7 – Experimental results and analysis of micro-truss parameter optimization.

Unit height A(mm)	Unit bottom side length B(mm)	Micro truss rod diameter C(mm)	Maximum temperature of cold surface R1(°C)	Maximum temperature of hot surface R2(°C)	Stiffness R3(N/mm)	Volume fraction(%)
3	4	8.0	63	100	5876527	31.06
3	4	1	69	99	9832960	34.63

3	3	0.9	74	99	13614249	36.26	
3	5	0.9	60	100	5286359	30.81	
5	4	0.8	54	100	3628740	22.12	
5	4	1	61	100	6153283	25.11	
5	3	0.9	68	100	8647673	26.9	
5	5	0.9	51	100	3246812	21.76	
4	3	0.8	66	99	8577998	28.51	
4	5	0.8	51	100	2860398	24.23	
4	3	1	73	99	26760806	33.04	
4	5	1	58	100	8886342	26.72	
4	4	0.9	62	100	5938607	27.28	

Use the response surface method to fit the cold surface maximum temperature, hot surface maximum temperature, stiffness and volume ratio in the table, and the regression equations of each response are obtained:

The highest temperature of cold surface:

$$R1 = 62 - 4A - 7.62B + 3.38C - 0.75AB + 0.25AC + 0.5A^{2} + 0.75B^{2} - 0.75C^{2}$$
(18)

Maximum temperature of hot surface:

$$R2 = 99.69 + 0.25A + 0.3750B - 0.125C \tag{19}$$

Stiffness:

$$R3 = 5.939 \times 10^{6} - 1.617 \times 10^{6} A - 4.665 \times 10^{6} B - 3.836 \times 10^{6} C - 7.318 \times 10^{5} AB$$

$$-3.58 \times 10^{5} AC - 3.039 \times 10^{6} BC - 1.819 \times 10^{6} A^{2} + 3.579 \times 10^{6} B^{2} + 2.253 \times 10^{6} C^{2}$$
(20)

Volume fraction:

$$R4 = 27.28A - 4.61A - 2.65B + 1.7C + 0.0775AB - 0.145AC - 0.51BC + 0.8788A^2 + 0.7738B^2 + 0.0712C^2$$
(21)

The response surface and contour lines of the interaction between unit cell height, unit cell bottom side length and micro-truss rod diameter on the maximum temperature of the cold surface are shown in Figure 10. The image shows that the maximum temperature of the cold surface decreases with the increase of unit height and unit bottom side length, and increases with the increase of rod diameter.

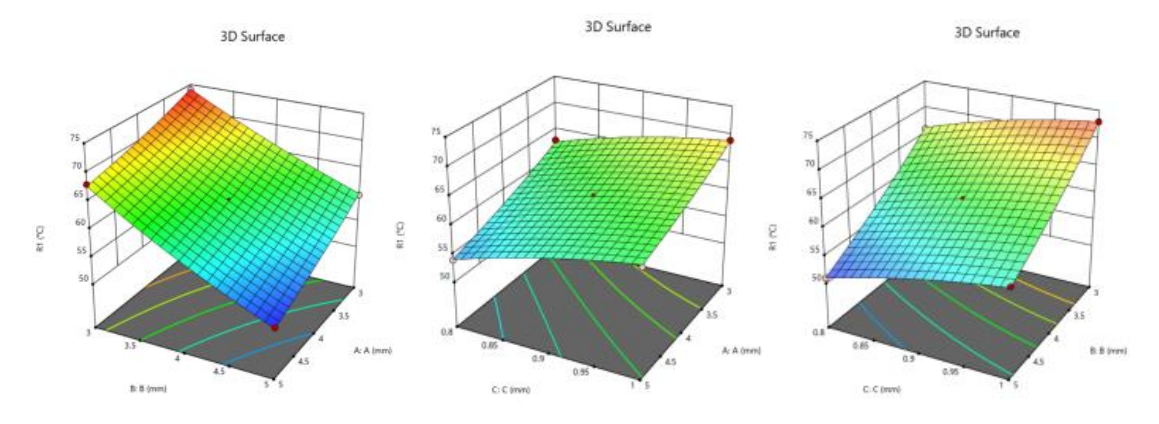


Figure 10 – Cold surface maximum temperature response surface.

The maximum temperature of the hot surface is basically maintained at around 100°C. This is because the hot surface temperature is less affected by the micro-truss and is mainly affected by the flow channel. The heat source of the hot surface transfers heat to the cold surface through the micro-truss area, so the size parameters of the micro-truss have a greater impact on the cold surface temperature.

The response surface and contour lines of the interaction between unit cell height, unit cell bottom side length and micro-truss rod diameter on stiffness are shown in Figure 11. The image shows that the stiffness decreases with the increase of element height and element bottom side length, and increases with the increase of rod diameter.

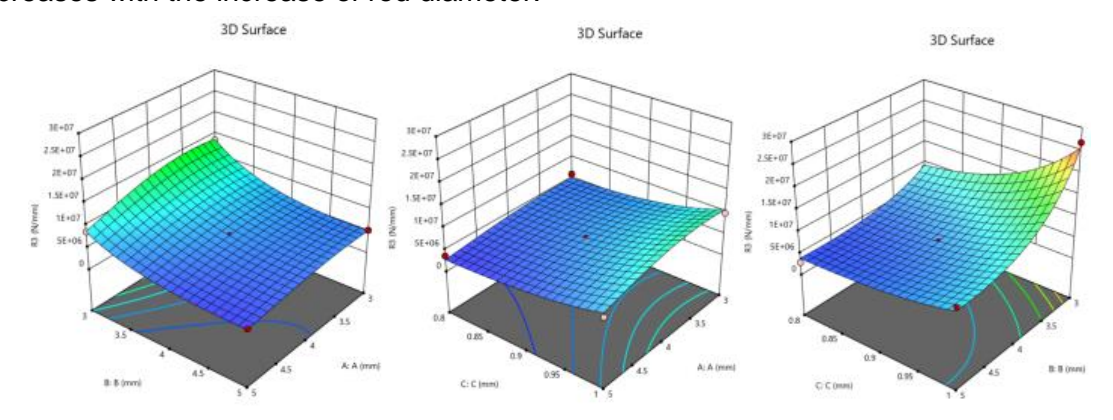


Figure 11 – Stiffness response surface.

When optimizing, the system transfers the established response surface expression to the optimization model, and adopts the MOGA multi-objective genetic optimization algorithm, namely NSGA-II, the second generation genetic algorithm of non-genetic dominance strategy. This method requires fewer samples to be calculated, and the feasible domain of the Pareto optimal solution can be obtained through analysis and calculation. The initial population generates 3000 samples, 600 samples per iteration, and the maximum allowed genetic generation is 20 generations, with a coefficient of variation of 0.01 and a crossover coefficient of 0.98. The maximum allowed Pareto ratio is set to 60%, and the convergence stability is set to 2%. After calculation by the multi-objective genetic algorithm and the Pareto method, the Pareto optimal solution is obtained. The optimal result is that the unit cell height A is 3.62mm, the unit cell bottom side length B is 5mm, and the micro-truss rod diameter C is 1mm.

3.3 Flow channel topology optimization

The topology optimization method based on Darcy flow [2]15 is used to optimize the flow channel in the leading edge plane area. The optimization formula is as follows:

min
$$\phi$$

s. t. $\left(\mathbf{K}_{t} + \mathbf{C}(\mathbf{p})\right)\mathbf{t} = \mathbf{f}_{t}$
 $\mathbf{K}_{p}\mathbf{p} = \mathbf{f}_{p}$

$$\sum_{i \in N_{e}} (1 - \hat{x})$$

$$g_{1} = \frac{\sum_{i \in N_{e}} (1 - \hat{x})}{(1 - V_{s})N_{e}} - 1 \le 0$$

$$g_{i} \le 0, i = 2 \cdots m$$

$$0 \le x_{i} \le 1, i = 1, 2 \cdots N$$
(22)

Among them, g1 is the volume constraint, and Vs is the volume fraction. m=3, indicating the number of constraints, g2 is the pressure drop constraint, and g3 is the geometric constraint. The objective function Φ is the maximum temperature in the plane area. Apply equation (20) to convert the objective function into a continuously differentiable form:

$$\phi = T_{\text{max}} \approx \left(\int_{\Omega^*} T^{\alpha} d\Omega \right)^{\frac{1}{\alpha}}$$
 (23)

In the formula, Ω is the design domain, T is the temperature, Tmax is the maximum temperature of the structure, and is a large constant, which is taken as 210 in this article.

The geometric and boundary condition characteristics of the front edge wall plate are extracted, the

wall plate is simplified into a 206mm*190mm plane model, and the flow channel topology is optimized. The design domain is shown in Figure 12. The heat source is distributed over the entire plane, with a linear gradient from 7750W/m2 near the entrance to 1550W/m2 near the exit. The inlet is 100ml/min of No. 65 coolant, the temperature is 300K, and the outlet pressure is 0.

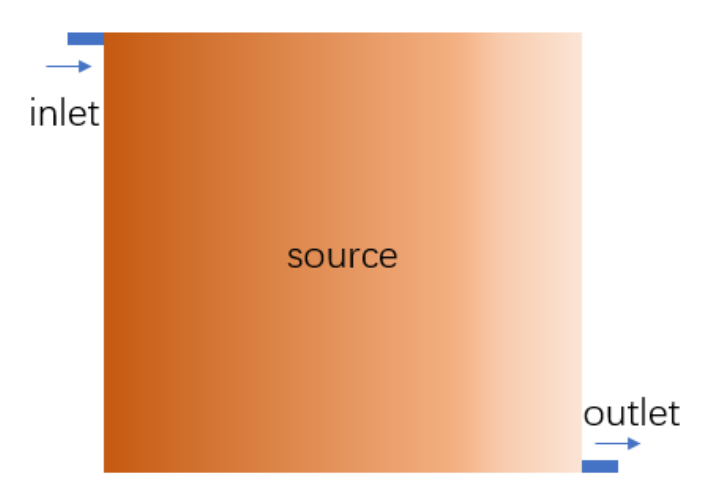


Figure 12 – Design Domain and Boundary Conditions.

After adjusting each parameter to appropriate values, the flow channel topology optimization results are obtained as shown in Figure 13.

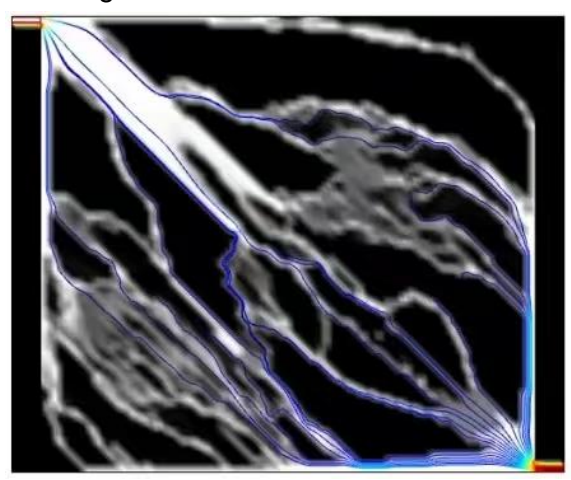


Figure 13 – Channel topology optimization results.

3.4 Evaluation of optimized structure

The active cooling structure at the leading edge of the aircraft designed in this article has an outer diameter of 12mm and an inner diameter of 6mm for the inlet and outlet pipes. The inlet pipe is directly connected to the front of the leading edge from one side to ensure that the low-temperature cooling medium first cools the hotter area at the front. The cooling medium passes through the flow channels in the upper and lower wall panels and finally flows to the other side of the opposite inlet, passing through the vertical pipe and intersecting with an outlet pipe. The shape of the flow channel is rectangular, and the micro-truss area adopts the optimized simple cubic unit, with a unit cell height A of 3.62mm, a unit cell bottom side length B of 5mm, and a micro-truss rod diameter C of 1mm. Due to thickness restrictions, the number of micro-truss unit filling layers is 1. The flow channel area uses topologically optimized flow channels and traditional direct current channels respectively, and analyzes the thermal protection effect of the embedded microstructure and the leading edge structure of the flow channel under given working conditions.

When a straight flow channel is used, the structural temperature cloud diagram and the flow

channel plane pressure cloud diagram are shown in Figure 14. The maximum temperature of the structure is 120°C, and the flow resistance is 93.6 MPa·s·m⁻³.

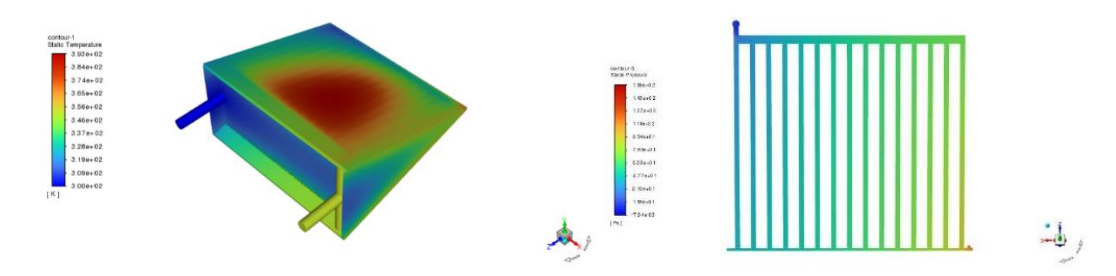


Figure 14 – Temperature and pressure cloud diagram of traditional direct current channel.

When the topology optimization flow channel is used, the structural temperature cloud diagram and the flow channel plane pressure cloud diagram are shown in Figure 15. The maximum temperature of the structure is 119°C, and the flow resistance is 67.8MPa • s • m⁻³.

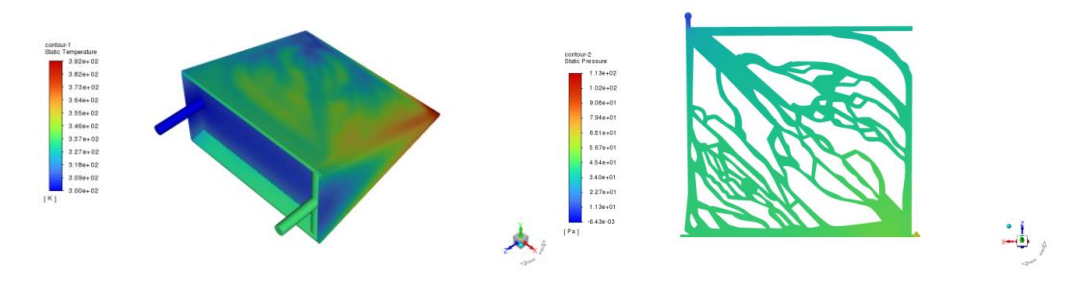


Figure 15 – Temperature and pressure cloud diagram of topology optimization flow channel.

The results show that the temperature of the topology optimized flow channel is lower than that of the traditional straight flow channel, the temperature distribution is more uniform, the heat dissipation effect is better, the flow resistance is smaller, and the safety is higher.

The temperature field calculated in the flow heat transfer simulation is retained, and a pressure load that gradually decreases linearly from 20MPa to 10MPa is applied to the outer wall of the leading edge to perform thermal-mechanical coupling simulation. The deformation and stress cloud diagram of the structure is shown in Figure 16. At this time, the maximum deformation is 0.14mm, which is relatively small, and the maximum stress is 673.5MPa, which is far less than the material strength limit.

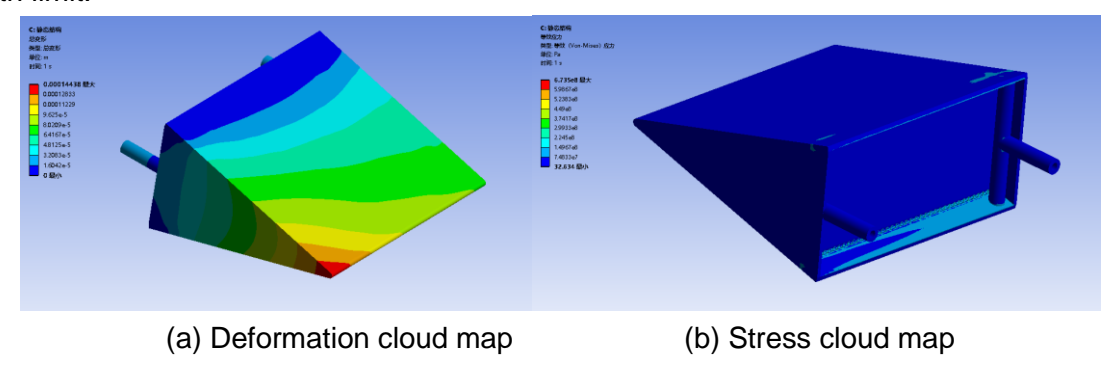


Figure 16 – Thermal-mechanical coupling simulation results.

4. Conclusions

In this paper, a dual-perspective approach aimed at enhancing load-bearing capacity and heat dissipation capabilities. The integration of lattice structures and cooling channels within the leading edge structure offers a promising solution.

Key findings from this study include:

- (1) Lattice structure: The specific stiffness, strength, and thermal conductivity of simple cubic (SC), body-centered cubic (BCC), and face-centered cubic (FCC) lattice structures were evaluated. These structures significantly improve the mechanical properties of the leading edge.
- (2) Cooling channel: Three cooling channels with different cross-sectional shapes (rectangular, triangular and semicircular) were studied, and the flow channel plan layout was topologically optimized. The rational design of these channels enhances the heat dissipation capability of the leading edge.
- (3) Simulation method: Use asymptotic homogenization method to reduce calculation time without sacrificing accuracy. This method has proven to be very effective, reducing the number of mechanical calculation grids and heat transfer calculation grids to 1% and 9% of the original model respectively, while maintaining high accuracy.
- (4) Response surface model: The response surface model was developed to establish the relationship between thermal and mechanical properties and the size of the lattice structure. The model facilitates multi-objective optimization of lattice designs, balancing stiffness and thermal performance.
- (5) Flow channel topology optimization: Based on the Darcy flow heat model, taking into account the maximum temperature, pressure drop and geometric constraints, a topology optimization model was created for the cooling channel. The optimized design exhibits superior heat dissipation performance compared to traditional designs, ensuring a more even temperature distribution across the entire front edge.

Simulation verification confirms the effectiveness of the proposed method. The optimized multiscale leading edge structure shows significant improvements in specific stiffness and heat dissipation efficiency, validating the design method proposed in this paper.

In conclusion, the methodology developed and applied in this study provides a powerful framework for the design of advanced leading edge structures capable of withstanding extreme service environments. The combination of lattice structure and optimized cooling channels, guided by rigorous computational and experimental analysis, enhances mechanical and thermal performance, contributing to aircraft safety and service life.

5. Contact Author Email Address

Mailto: pingxu@email.cn

6. Copyright Statement

The authors confirm that they, and/or their company or organization, hold copyright on all of the original material included in this paper. The authors also confirm that they have obtained permission, from the copyright holder of any third party material included in this paper, to publish it as part of their paper. The authors confirm that they give permission, or have obtained permission from the copyright holder of this paper, for the publication and distribution of this paper as part of the ICAS proceedings or as individual off-prints from the proceedings.

References

- [1] Rosario B., Aniello R., Domenico Tescione. Thermo-structural behaviour of an UHTC made nose cap of a reentry vehicle[J]. *Acta Astronautica* 2009 (65): 42–456.
- [2] JIN X, LI Y, YAN H, et al. Comparative study of flow structures and heat transfer enhancement in a metallic lattice fabricated by metal sheet folding: effects of punching location shift [J]. *International Journal of Heat and Mass Transfer*, 2019, 134: 209-225.
- [3] WADLEY H N G. Multifunctional periodic cellular metals[J]. *Philosophical Transactions of the Royal Society A:Mathematical, Physical and Engineering Sciences*, 2006, 364 (1838) : 31-68.
- [4] KHADERI S N,DESHPANDE V S,FLECK N A.The stiffness and strength of the gyroid lattice[J]. *International Journal of Solids and Structures*, 2014, 51(23-24):3866-3877.
- [5] VALDEVIT L, HUTCHINSON J W, et al. Structurally optimized sandwich panels with prismatic cores[J]. *International Journal of Solids and Structures*, 2004, 41(18-19):5105-5124.
- [6] MOON S K,TAN Y E,HWANG J. Application of 3D printing technology for designing light-weight unmanned aerial vehicle wing structures[J]. *International Journal of Precision Engineering and Manufacturing-Green Technology*, 2014,1(3):223-228.
- [7] ZHU Y, PENG W, XU R, et al. Review on active thermal protection and its heat transfer for airbreathing hypersonic vehicles[J]. *Chinese Journal of Aeronautics*, 2018, 31(10): 1929-1953
- [8] Xiang, S. H., M. J. Zhang, and JY TONG. "Research on active film cooling and heat-proof scheme for hypersonic vehicles." *Equipment Environmental Engineering* 12.3 (2015): 1-7.
- [9] J.V. Becker, New Approaches to Hypersonic Aircraft, in: 7th International Council of the Aeronautical Sciences, ICAS Paper, Rome, Italy, 1970, p. 70, 16.
- [10]WIETING A R,DECHAUMPHAI P,BEY K S, et al. Application of integrated fluid -thermal-structural analysis methods[J]. *Thin-Walled Structures*,1991,11 (1/2):1-23.
- [11]SCOTTI S J, MARTIN C J, LUCAS S H. Active cooling design for scramjet engines using optimization methods[R]. *AIAA* 88-2265,1988.
- [12]YOUN B, MILLS A F. Cooling panel optimization for the active cooling system of a hypersonic aircraft[J]. *Journal of Thermophysics and Heat Transfer*,1995,9 (1):136-143.
- [13]Samson, Sean, Phuong Tran, and Pier Marzocca. "Design and modelling of porous gyroid heatsinks: Influences of cell size, porosity and material variation." *Applied Thermal Engineering* 235 (2023): 121296.
- [14]Li, Quhao, et al. "Topology optimization design of quasi-periodic cellular structures based on erode—dilate operators." *Computer Methods in Applied Mechanics and Engineering* 377 (2021): 113720.
- [15]Zhao, Xi, et al. "A "poor man's approach" to topology optimization of cooling channels based on a Darcy flow model." *International Journal of Heat and Mass Transfer* 116 (2018): 1108-1123.
- [16] Forsberg J, Nilsson L. Evaluation of response surface methodologies used in crashworthiness optimization [J]. *International journal of impact engineering*, 2006, 32(5): 759-777.
- [17]Xiang Y, Wang Q, Fan Z, et al. Optimal crashworthiness design of a spot-welded thin-walled hat section[J]. *Finite Elements in Analysis and Design*, 2006, 42(10): 846-855.